Promoting effect of AuCu alloying on Au-Cu/CeO 2 -catalyzed CO oxidation: A combined kinetic and in situ DRIFTS study

Xuemei Liao, Yanmin Liu, Wei Chu, Sécou Sall, Corinne Petit, Véronique Pitchon, Valérie Caps

Journal of Catalysis 382 (2020) 329–338

Contents lists available at ScienceDirect

Journal of Catalysis

journal homepage: www.elsevier.com/locate/jcat

Promoting effect of AuCu alloying on Au-Cu/CeO_2-catalyzed CO oxidation: A combined kinetic and in situ DRIFTS study

Xuemei Liao [a,b,c], Yanmin Liu [a], Wei Chu [b], Sécou Sall [c], Corinne Petit [c], Véronique Pitchon [c], Valérie Caps [c,*]

[a] College of Food and Biological Engineering, Xihua University, Chengdu 610039, China
[b] Department of Chemical Engineering, Sichuan University, Chengdu 610065, China
[c] ICPEES, Institut de Chimie et Procédés pour l'Energie, l'Environnement et la Santé, Université de Strasbourg, CNRS UMR 7515, 25 Rue Becquerel, 67087 Strasbourg, France

ARTICLE INFO

Article history:
Received 6 November 2019
Revised 19 December 2019
Accepted 20 December 2019
Available online 20 January 2020

Keywords:
Bimetallic nanoparticles
Gold catalysis
AuCu nanoalloy
CO oxidation
PROX

ABSTRACT

Reduced Au-Cu/CeO_2 catalysts (Cu/Au = 1, 3) are more efficient towards the preferential oxidation of CO (PROX) than their calcined counter-parts. They exhibit lower activation energies and CO partial reaction orders (α_{CO}), and even more interestingly, significantly higher O_2 partial reaction orders (β_{O2}). For the stoichiometric composition in particular (Au_1Cu_1/CeO_2-R), the partial pressure of oxygen has a higher impact on the reaction rate than the partial pressure of CO ($\beta_{O2} > \alpha_{CO}$), which is unprecedented in low temperature catalysis involving gold and a reducible oxide support. DRIFTS studies further show (1) that Au_1Cu_1/CeO_2-R contains electron-deficient, alloyed Cu atoms (Au-Cu^+) and (2) that the formation of CO_2 is enhanced by the preadsorption of O_2 rather than the preadsorption of CO. This suggests that CO oxidation proceeds *via* a Langmuir-Hinshelwood-type, bifunctional mechanism, involving CO adsorbed on Au^0 sites and oxygen adsorbed on electron-deficient, gold-alloyed copper sites. This alloy-mediated oxygen activation could be the key to the superior PROX activity of Au_1Cu_1/CeO_2-R.

1. Introduction

The ability to oxidize CO at room temperature is of great importance for the purification of indoor and outdoor air (CO oxidation), as well as for the purification of hydrogen fuels feeding polymer exchange membrane fuel cells (CO preferential oxidation, CO-PROX). In this regard, supported Au-Cu bimetallic catalysts [1–14] have attracted much attention in recent years because they may, under certain conditions, exhibit superior catalytic activity in CO oxidation as compared to the Au and Cu monometallic catalysts. In particular, significant improvement in CO-PROX light-off temperatures was observed in ceria-supported AuCu [4,5,7,8] when the samples were reduced. Amongst reduced catalysts, the stoichiometric Cu/Au composition, Au_1Cu_1/CeO_2-R, exhibited the largest improvement. The improvement in CO conversion was much larger than the one that could be expected from the higher dispersion of gold in the reduced sample, as compared with the calcined ones, and from a possible size effect. Alloy formation was speculated to account for the higher activities observed, but no insight in the molecular processes involved in the mechanism was given [4].

Combining diffuse reflectance infrared Fourier transform (DRIFT) spectroscopy and kinetic studies could be helpful for that purpose. There is currently no available kinetic data on the AuCu-catalyzed CO oxidation and no available DRIFT study on the ceria-supported AuCu system. However, DRIFTS has proven useful for investigating the mechanism of the CO oxidation reaction on Au/CeO_2 [15–20], Cu/CeO_2 [21–28], and bimetallic AuCu [2,3,6,11] supported on "inert" supports according to Schubert's classification of supports for gold-catalyzed CO oxidation [29], namely alumina and silica. For Cu/CeO_2 catalysts, CO oxidation rates were shown to correlate well with the formation of Cu^+–CO [21,23] and to follow a Mars-Van Krevelen mechanism involving the redox properties of ceria in oxygen activation [26,30]. For Au/CeO_2 and silica-supported AuCu catalysts, Au^0 was found to be the most relevant site regarding CO adsorption and oxidation [3,31]. Boccuzzi et al. reported that CO and O_2 were competitively adsorbed on these Au sites supported on TiO_2 at 91 K [18,32] and that oxygen could also be activated on an oxygen vacancy of the support close to the gold nanoparticles [20]. Such a two-site model of non-competitive adsorption, CO adsorbing on Au and O_2 adsorbing on the support (e.g. TiO_2) [19], is generally accepted

* Corresponding author.
E-mail address: caps@unistra.fr (V. Caps).

https://doi.org/10.1016/j.jcat.2019.12.029
0021-9517/

for supported gold catalysts exhibiting Langmuir-Hinshelwood kinetics [16].

Concerning the kinetics of the Cu/CuO-CeO_2 [33–37] and Au-catalyzed [38–44] CO-PROX reactions, it has been shown that copper-catalyzed reactions exhibited high values of apparent activation energies (Ea), from 50 to 100 kJ/mol, whereas gold-catalyzed reactions exhibited much lower Ea with values of 20–40 kJ/mol. Besides, for supported Au catalysts, the partial reaction orders of both CO (α) and O_2 (β) for supported Au are positive. Generally, $\beta_{O2} \sim \alpha_{CO}$ when Au nanoparticles (NP) are associated with "inert" supports [44] and $\beta_{O2} < \alpha_{CO}$ when Au NP are associated with reducible supports [38,39].

The aim of this work is to provide a kinetic study of the AuCu/CeO_2-catalyzed CO oxidation in the presence of hydrogen and DRIFT analysis of the adsorption of CO in the absence and in the presence of O_2 (reactive atmosphere), for both calcined (AuCu/CeO_2-C) and reduced (AuCu/CeO_2-R) systems. The correlation between these two studies is shown to bring new mechanistic insight in the otherwise highly documented Au-catalyzed CO oxidation. The mechanistic aspects of CO oxidation on the optimum formulation of Au_1Cu_1/CeO_2-R are further considered, in comparison with monometallic and calcined catalysts. A new site for oxygen activation is proposed. It is expected to be involved in the alloy-catalyzed oxidation of CO regardless of the presence or the absence of hydrogen.

2. Experimental

2.1. Catalyst preparation

The bimetallic Au_xCu_y/CeO_2 catalysts were prepared by a two-step method, as previously described [4,9]. First, gold was loaded on ceria using Direct Anionic Exchange (DAE) [45,46]. Copper was then loaded on the resulting Au-CeO_2 powder by impregnation (IMP) after introduction of Au-CeO_2 into an aqueous solution of Cu $(NO_3)_2{\cdot}3H_2O$ and stirring for 3 h, the solution was evaporated and the remaining solid dried in an oven at 110 °C for 3 h. The gold loading was fixed at 2 wt% and the amount of copper was chosen in order to vary the atomic Au/Cu ratio (Au/Cu = 1:3 and 1:1).

A fraction of the catalyst precursor was calcined under air by heating to 300 °C at 4 °C/min and holding at 300 °C for 4 h. The other fraction of the catalyst precursor was reduced in a furnace under a flowing 50% H_2/He gas mixture with a flow rate of 50 mL/min^{-1}, holding at 300 °C for 2 h. The obtained samples were named according to the nominal Cu/Au atomic ratio and the post-synthesis treatment applied (C or R for calcination or reduction, respectively), as follows: Au_1Cu_1/CeO_2-C, Au_1Cu_1/CeO_2-R, Au_1Cu_3/CeO_2-C and Au_1Cu_3/CeO_2-R.

For comparison, monometallic Au/CeO_2-C and CuO/CeO_2-C catalysts were prepared by analogous DAE and IMP methods and finally calcined at 300 °C for 4 h. The targeted loading of Au or Cu was 2 wt%. Reduced monometallic catalyst (Au/CeO_2-R and CuO/CeO_2-R) were also prepared for the FTIR study, using the same hydrogen treatment as the one used for bimetallic catalysts.

Basic characterization (ICP, H_2-TPR, XRD, XPS, HRTEM) and activity measurements (light-off curves) of all the materials may be found elsewhere [4]. In brief, all catalysts contain 2.10 ± 0.05 wt% Au with average size 2.0 ± 0.5 nm in the reduced catalysts and 3.0 ± 0.5 nm in the calcined materials. Copper content varies from 0.80 wt% to 1.86 wt% and 1.94 wt% in Au_1Cu_1/CeO_2, Au_1Cu_3/CeO_2 and Cu/CeO_2, respectively.

2.2. Kinetic measurements

Catalytic kinetics of CO preferential oxidation was studied at atmospheric pressure in a quartz micro-reactor. Catalysts were diluted 1:20 (wt./wt.) with cordierite. The catalyst mass was fixed at 0.005 ± 0.001 g except in the case of CuO/CeO_2, where a mass of 0.02 g was used. The gas mixture ($CO/O_2/H_2$ balanced by He) was introduced at a flow rate of typically 200 mL/min, which allowed to obtain very low CO conversion and maintained the catalysts under kinetic control. The flow rate was controlled using Tylan mass flow controllers. The temperature (T) was monitored and controlled by a Eurotherm system. Analyses of CO, O_2 and CO_2 were performed using a Rosemount Infrared analyzer. Parameters were varied in the following ranges: 25 °C < T < 180 °C; P_{H2} = 50 kPa; P_{CO} = 0.25, 0.5, 1, 1.5 kPa (with P_{O2} = 1 kPa); P_{O2} = 0.25, 0.5, 1, 1.5 kPa (with P_{CO} = 1 kPa). The CO conversion (X_{CO}) and CO oxidation rates (r, $mmol_{CO}/s/g_{cat}$) were calculated using $X_{CO} = \frac{[CO_2]out}{[CO]in}$ and $r = \frac{F \times C_{CO} \times X_{CO}}{22.4} \times \frac{1}{60} \times \frac{T_0}{T} \times \frac{1}{m_{cat.}}$ with F = total flow rate of the reactants; C_{CO} = CO concentration; T_0 = 298 K; m_{cat} = catalyst mass. CO and O_2 partial reaction orders, α_{CO} and β_{O2}, respectively, were calculated from $r = kP_{CO}^{\alpha}P_{O2}^{\beta}$. Apparent activation energies (E_a) were calculated using the Arrhenius law: $r = A.\exp[-E_a/RT]$.

2.3. In situ diffuse reflectance FTIR (DRIFTS) measurements

The in situ diffuse reflectance FTIR spectra were collected on a Bruker VERTEX 70 spectrometer equipped with a MCT (HgCdTe) detector with a 4 cm^{-1} spectral resolution. In each experiment, the powder samples in form of raw powder without KBr were introduced in a Praying Mantis™ low temperature reaction chamber from Harrick Scientific (model No CHC-CHA-3, cell volume of about 12 cm^3), allowing thermal treatment in controlled atmospheres and spectrum scanning at controlled temperatures (from −90 °C up to room temperature (RT)). Before adsorption experiments and catalytic tests, the previously calcined or reduced catalysts (about 80 mg) were submitted to an oxidative or reductive pretreatment in situ to remove the impurities and moisture from catalyst surfaces. Oxidative treatment consisted in heating from RT up to 150 °C with a rate of 10 °C/min, inlet of air with a flow rate of 5 mL/min, and then holding at 150 °C for 2 h. After that, the sample was cooled down to room temperature in oxygen atmosphere and finally continued to cool down to −90 °C using liquid nitrogen under vacuum. Reductive treatment consisted in heating from RT up to 150 °C with a rate of 10 °C/min, inlet of pure hydrogen with a flow rate of 5 mL/min, and then holding at 150 °C for 2 h. After that, the sample was cooled down to room temperature in hydrogen atmosphere and finally continued to cool down to −90 °C using liquid nitrogen under vacuum. The chemisorption of CO and CO oxidation was performed at −90 °C unless otherwise mentioned, using a transient gas switching system. For the chemisorptions of CO, a 4% CO/He gas mixture, i.e. 30 Torr CO, was used and let to equilibrate with the catalyst surface. Spectra corresponding to maximum CO chemisorptions were used for discussion, unless otherwise mentioned. From each spectrum, the spectrum of the sample before the inlet of CO (background spectrum) was subtracted. Oxidation reactions were performed with an additional 20% O_2/He gas mixture. Relative intensities of adsorbed CO and CO_2 species are defined as $I_{COad}(t)/I_{COad}(t_0)$ and $I_{CO2ad}(t)/I_{CO2ad}(t_0)$, respectively, where I is the intensity of the FTIR band, COad and CO_2ad stand for the adsorbed species, t0 stands for the spectrum obtained before switching gases, t stands for spectra obtained at any given time t after the gas switch. All spectra have been normalized by the exact weight of the powders (about 80 mg).

3. Results and discussion

Activity and stability of the catalysts were previously established [4].

3.1. Reaction kinetics

3.1.1. Activities and activation energies

Apparent activation energies for PROX (Table 1) were determined from the plots which consist in linear regressions of the logarithms of the reaction rates vs. the inverse of the reaction temperatures (Fig. 1). The linear regressions were obtained with a coefficient of determination R^2 above 0.99. An error of ±3 kJ/mol applies to the apparent activation energy values summarized in Table 1.

Monometallic Au/CeO_2 and CuO/CeO_2 catalysts show apparent activation energies around 40 and 83 kJ/mol, respectively, which are consistent with previously reported values of Au/Al_2O_3 prepared by the same DAE method (≈38 kJ/mol) [44] and for CuO/CeO_2 (≈83 kJ/mol) [34], respectively. Hence CO oxidation proceeds much more easily on the gold catalyst than on the copper one, in agreement with previous activity reports [4]. Interestingly, the inclusion of Cu in the reduced catalysts (Au_1Cu_1/CeO_2-R and Au_1Cu_3/CeO_2-R) has almost no effect on the activation energy of Au/CeO_2 (Fig. 1). For all bimetallic materials, the apparent activation energy is lower than that previously observed for CuO/CeO_2. It decreases to 65 and 46 kJ/mol for the calcined and reduced copper-rich materials, respectively, and further to 50 and 41 kJ/mol for the calcined and reduced materials, respectively, by decreasing the copper content down to the stoichiometric composition. At both Cu/Au ratios of 3 and 1, apparent activation energies are lower for the reduced materials as compared to their calcined counter-parts. By decreasing the energy barrier, the reduction pretreatment thus facilitates CO oxidation. However, activation energies observed over reduced Au-Cu/CeO_2 catalysts are similar to that observed over Au/CeO_2. The higher mass-specific reaction rate of Au_1Cu_1/CeO_2-R (Table 1) can thus not be solely explained on the basis of reaction barriers, and further insight into kinetics of the reaction is needed.

3.1.2. Reaction orders

The reaction order with respect to CO was determined by keeping the partial pressure of O_2 constant at 1 kPa and varying the partial pressure of CO (Fig. 2). Next, the reaction order of O_2 was determined by keeping the partial pressure of CO constant at 1 kPa and varying the partial pressure of O_2 (Fig. 3). This was performed at three different temperatures (100 °C, 120 °C and 150 °C). For each temperature, the logarithmic dependence of the reaction rate versus partial pressure of each reactant is plotted. The CO and O_2 partial orders (Table 2) are calculated from the linear regression of the plots. For all catalysts, CO and O_2 reaction order are positive and vary to a more or less significant extent with the temperature.

3.1.2.1. Monometallic systems. For the monometallic Au/CeO_2-C catalyst, reaction orders with respect to CO and O_2, α_{CO} and β_{O2} respectively, both increase with increasing temperature. This is in good agreement with a previously reported increase in CO reaction order over Au/TiO_2, from 0.2 to 0.6 as the temperature increased from 37 to 87 °C [47]. Besides, at each of the temperatures studied, the reaction order with respect to CO is systematically and significantly higher than the reaction order with respect to O_2. This shows that the CO oxidation rate is much more dependent on the concentration of CO than on the concentration of O_2. Similar results were obtained by Kahlich *et al.*, who reported

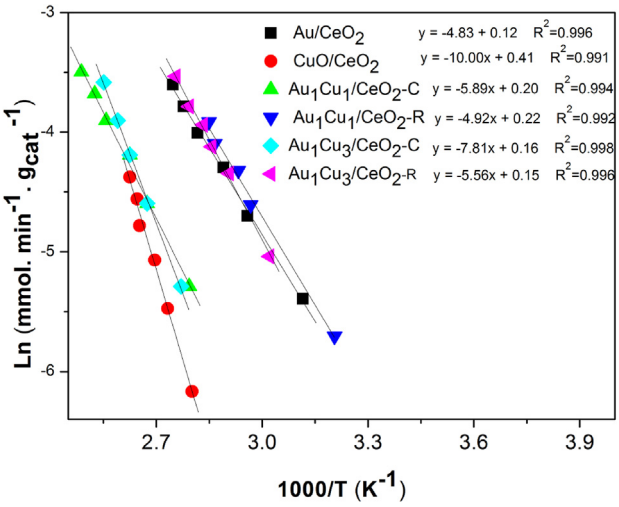

Fig. 1. Determination of apparent activation energies using 1 kPa CO, 1 kPa O_2 and 50 kPa H_2 in He.

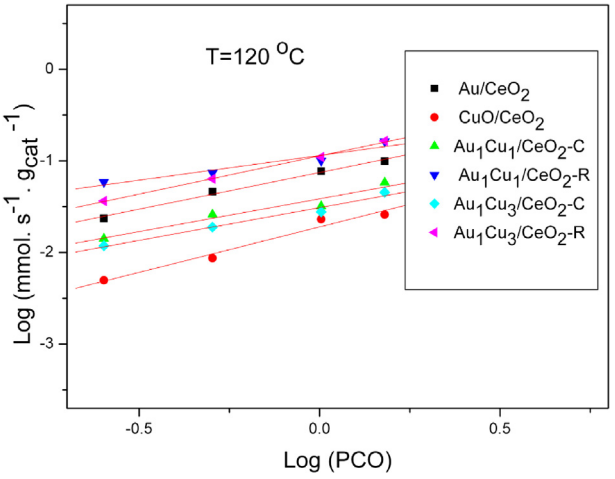

Fig. 2. Determination of the carbon monoxide partial reaction orders (α_{CO}) at 120 °C, P_{O2} = 1 kPa. Measurements were performed at increasing CO pressure.

Table 1
Apparent activation energies, pre-exponential factors and reaction rates.

Catalyst	E_a (kJ/mol)[a]	E_a (kJ/mol)[b]	Pre-exponential factor		Mass-specific reaction rate[c]	
			ln(A)	A	($mol_{CO}.s^{-1}.g_{\bar{A}u}^{-1}$)	($mol_{CO}.s^{-1}.g_{\bar{A}uCu}^{-1}$)
Au/CeO_2-C	40	42	0.12	1.13	1.70	1.70
CuO/CeO_2-C	83	81	0.41	1.51	0.31	0.31
Au_1Cu_1/CeO_2-C	50	48	0.20	1.22	0.38	0.27
Au_1Cu_3/CeO_2-C	65	63	0.16	1.17	0.50	0.26
Au_1Cu_1/CeO_2-R	41	42	0.21	1.23	2.99	2.13
Au_1Cu_3/CeO_2-R	46	45	0.15	1.16	2.27	1.17

[a] Apparent activation energy under 1 kPa CO, 1 kPa O_2 and 50 kPa H_2 in He.
[b] Apparent activation energy under 0.5 kPa CO, 1 kPa O_2 and 50 kPa H_2 in He.
[c] Calculated at 100 °C.

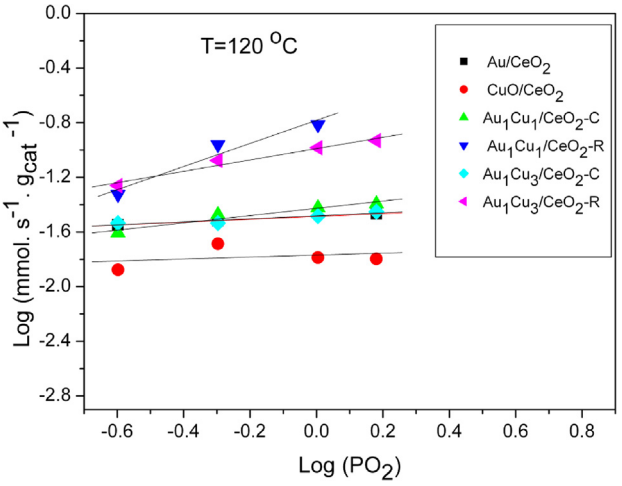

Fig. 3. Determination of the oxygen partial reaction orders at 120 °C, P_{CO} = 1 kPa. The measurements were performed from low to high pressures. Note that these measurements were carried out after determination of the CO partial reaction order.

that the CO oxidation rate over Au/Fe_2O_3 was strongly dependent on the partial pressure of CO, but weakly dependent on the partial pressure of O_2 (α_{CO} = 0.55, β_{O2} = 0.27 at 80 °C) [38]. A Langmuir-Hinshelwood mechanism is generally proposed to fit these kinetic data, in which CO is activated on the gold nanoparticle and oxygen is activated at the metal-support interface [16,29,38,48]. It is noted that similar kinetic results were found over Au/CeO_2 in the absence of hydrogen (α_{CO} = 0.3, β_{O2} = 0.18 at T < 60 °C) [49], showing that the mechanism of CO oxidation over Au/CeO_2 is not significantly impacted by the presence of hydrogen. Ceria-supported gold catalysts indeed exhibit similar CO oxidation rates in hydrogen-free and hydrogen-rich mixtures [50].

For the monometallic CuO/CeO_2-C catalyst, the difference between the CO and O_2 partial reaction orders is even more significant. Partial reaction orders with respect to CO are larger than those found on the gold catalyst, while the O_2 partial reaction orders are lower, close to zero at 100 and 120 °C. On the copper catalyst, the reaction rates below 120 °C are thus quasi-independent from the partial pressure of O_2, and more strongly determined by the partial pressure of CO, than on gold catalysts. Similar CO partial reaction orders (<1 for temperatures below 110 °C, >1 for temperatures above 110 °C) have been reported in other studies of the CuO/CeO_2-catalyzed PROX reaction [34,35]. It is interesting that in the absence of hydrogen, the CO reaction order is significantly lower: values of 0.36 ± 0.1 have been reported in the 30–80 °C temperature range [37]. In addition to the presence of hydrogen, the higher reaction temperature, the lower Cu content and/or the milder thermal treatment of our catalyst may also contribute to the higher CO partial reaction order found here (0.85 at 100 °C). Regarding the O_2 partial reaction order, values close to zero are generally reported for the Cu-CeO_2 system at temperatures below 120 °C, regardless of presence or absence of hydrogen in the feed [34,35,37]. This is generally consistent with the occurrence of a Mars-Van Krevelen mechanism and the involvement of lattice oxygen species from the bulk oxide at low temperature [37,51,52]. At higher temperatures, the partial pressure of oxygen has a more significant impact on the CO oxidation rate: at 150 °C, the O_2 partial reaction order indeed becomes significant with a value close to that observed over the gold catalyst at this temperature (Table 1). This is attributed to enhanced activation of gas phase oxygen on oxygen vacancies and to enhanced oxygen diffusion within the bulk.

3.1.2.2. Bimetallic systems. For bimetallic catalysts, O_2 reaction orders are significantly higher than those found on either of the monometallic catalysts, whatever the temperature considered, reaching 0.97 for Au_1Cu_1/CeO_2-R (Table 1). β_{O2} generally decreases with increasing copper content and is systematically higher on the reduced catalyst than on the calcined one. On the other hand, CO reaction orders are generally much lower than those found on Cu/CeO_2 and Au/CeO_2. α_{CO} generally increases with increasing copper content. Comparing O_2 and CO partial reaction orders on the bimetallic catalysts, it appears that the O_2 partial orders remain lower than the CO partial orders, like for the monometallic catalysts. However, one notable exception to that is displayed by Au_1Cu_1/CeO_2-R. Indeed, not only does this catalyst exhibit the highest β_{O2} of the series, at all considered temperatures, but it is also the only catalyst for which β_{O2} is markedly superior to α_{CO} (for T < 120 °C). In particular, at 100 °C, the main difference between Au/CeO_2 and Au_1Cu_1/CeO_2-R is the much larger dependence of the bimetallic-catalyzed reaction rate on the O_2 partial pressure. Such high oxygen reaction orders have never been reported for either the Au- or the Cu-catalyzed low temperature PROX reaction. Only a few examples of gold-based catalysts have been found to display such a high oxygen reaction order in high temperature, hydrogen-free CO oxidation, such as $AuNi/TiO_2$ systems with Ni/Au > 0.6 [53], Au/SiO_2 and $AuPt/SiO_2$ systems with Au/Pt = 1.8 [54]. The positive difference in O_2 and CO reaction orders also can be found in high temperature CO oxidation [54], in which oxygen activation is the rate-determining step. On the other hand, the CO reaction orders are similar for both Au/CeO_2 and Au_1Cu_1/CeO_2-R, which suggests that the activation of CO is unmodified by the presence of Cu. Hence, the activation of CO likely occurs on similar sites in both Au/CeO_2 and Au_1Cu_1/CeO_2-R.

3.1.3. Summary

Low temperature PROX catalyzed by bimetallic Au-Cu/CeO_2 catalysts is thus characterized by (1) an activation energy in-between that of the Au/CeO_2-catalyzed process and that of the Cu/CeO_2-catalyzed process, (2) a CO reaction order in-between that of the Au/CeO_2-catalyzed process and that of the Cu/CeO_2-catalyzed process, (3) a higher dependence on the oxygen partial pressure than both the Au/CeO_2- and Cu/CeO_2-catalyzed processes. For the calcined materials, the reaction rate remains significantly more dependent on the CO than on the O_2 partial pressure, and CO

Table 2
Reaction orders.

Catalyst	P_{CO} (kPa)	P_{O2} (kPa)	100 (°C)		120 (°C)		150 (°C)	
			α_{CO}	β_{O2}	α_{CO}	β_{O2}	α_{CO}	β_{O2}
Au/CeO_2-C	0.25–1.5	0.25–1.5	0.34	0.11	0.80	0.15	1.08	0.52
CuO/CeO_2-C	0.25–1.5	0.25–1.5	0.85	0.02	0.99	0.07	1.18	0.44
Au_1Cu_1/CeO_2-C	0.25–1.5	0.25–1.5	0.72	0.33	0.71	0.26	0.84	0.52
Au_1Cu_3/CeO_2-C	0.25–1.5	0.25–1.5	1.03	0.30	0.72	0.11	0.91	0.62
Au_1Cu_1/CeO_2-R	0.25–1.5	0.25–1.5	0.38	0.55	0.54	0.84	1.03	0.97
Au_1Cu_3/CeO_2-R	0.25–1.5	0.25–1.5	0.58	0.45	0.83	0.42	1.02	0.83

activation may thus be considered as the rate-determining step, like in the Au/CeO_2- and Cu/CeO_2-catalyzed processes. The significantly higher O_2 reaction orders suggest that the Au/CeO_2 interface may be fully blocked/occupied by the copper oxide phase, and that, as a result, oxygen activation may be displaced from the ceria support to the copper phase. In other words, the reaction between adsorbed CO (on both Au and Cu) and adsorbed O_2 (on ceria) likely proceeds on the copper phase in the absence of direct and available interface between Au and CeO_2. For the reduced catalysts, the difference in CO and O_2 reaction orders is much smaller. It even becomes negative for the stoichiometric Au_1Cu_1 composition with the superior activity. The reduction seems key in exerting a synergistic effect from Au and Cu. The switch from $\beta_{O2} < \alpha_{CO}$ to $\beta_{O2} > \alpha_{CO}$ appears to be the key to an optimized oxygen activation pathway. It is associated with an activation energy and CO reaction order similar to Au/CeO_2, which suggests that Cu decorates the catalyst surface in a manner that is specific enough not to disturb CO activation on gold and that allows fast reaction between CO and O_2.

3.2. Infrared investigation

In order to gain more information at a molecular level about adsorption sites, active sites, and nature of the active reactants (adsorbed vs. gas phase), DRIFTS measurements were performed under different conditions.

3.2.1. Comparative study of CO adsorption

The infrared spectra of CO adsorption on monometallic and bimetallic Au-Cu catalysts are shown in Figs. 4 and 5, respectively. The calcined Au/CeO_2-C catalyst exhibits a signal with two maxima at 2103 and 2117 cm^{-1} (Fig. 4). The less intense peak at 2103 cm^{-1} is typical of CO adsorbed on metallic gold, Au^0-CO [55]. It has been observed on gold nanoparticles supported on various oxides. It has been found to be quite independent from the support, so that the adsorption sites are generally proposed to be on top of the gold particle. The more prominent peak at 2117 cm^{-1} is attributed to CO co-adsorbed on a step site with atomic oxygen (O-Au-CO) [56]. It is interesting that this band at 2117 (±2) cm^{-1} is generally observed on gold catalysts supported on reduced ceria [57] or titania, *after* oxygen is introduced on pre-adsorbed CO. Hence the presence of this band upon simple CO adsorption on Au/CeO_2-C suggests that the Au-O sites arise from the interaction between the gold particle and oxygen from the fully oxidized support [57]. The adsorption site related to the 2117 cm^{-1} vibration is thus

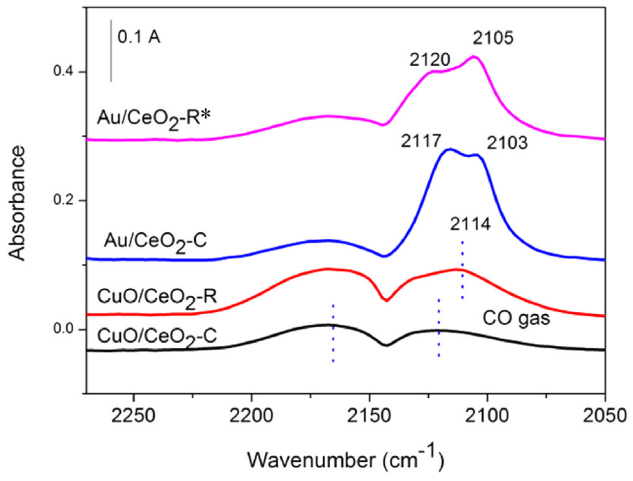

Fig. 4. FTIR spectra of CO adsorption (4%CO/He, −90 °C) on monometallic, ceria-supported gold and copper catalysts. Au/CeO_2-R* is obtained from Au/CeO_2-C by hydrogen (5 mL/min) treatment in the DRIFT cell at 150 °C for 2 h.

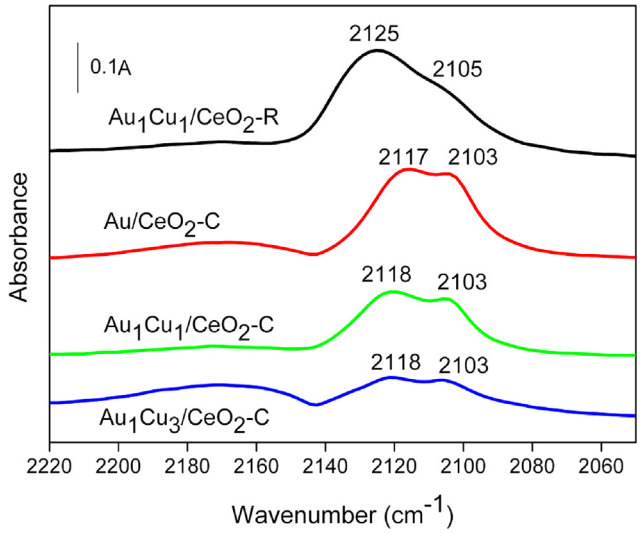

Fig. 5. FTIR spectra of CO adsorption (4%CO/He, −90 °C) on ceria-supported bimetallic gold-copper catalysts.

ascribed to a perimeter site of the gold particle. It is noted that, the position of CO adsorbed on cationic $Au^{\delta+}$ is expected in the 2130–2175 cm^{-1} range [31,32,55,58–61], the wavenumber increasing with increasing oxidation state of gold, up to 2175 cm^{-1}, for CO adsorbed on Au^{III}. No such signal is observed here (Fig. 4), showing the absence of such oxidized gold species in our samples. The catalyst reduced at 150 °C, Au/CeO_2-R*, also exhibits a two-component signal spreading from 2080 to 2140 cm^{-1} with maxima at 2105 and 2120 cm^{-1} (Fig. 4). The main difference with Au/CeO_2-C is the relative ratio of the low vs. high wavenumber component intensities: in Au/CeO_2-R*, the component attributed to Au^0-CO (2105 cm^{-1}) [55] is more prominent than the component attributed to the peripheral O-Au-CO species (2120 cm^{-1}). This suggests that the number of oxygen atoms present on the peripheral sites of the Au NP is smaller in Au/CeO_2-R* than in Au/CeO_2-C, in agreement with the blue shift (+3 cm^{-1}) observed in the position of the high wavenumber component, as compared with its position in the calcined gold catalyst. The most likely explanation is that, in Au/CeO_2-R*, the ceria support is at least partially reduced by the hydrogen treatment at 150 °C and that this reduction has occurred in the direct vicinity of the gold particle, due to noble metal-promoted reduction [62]. A number of oxygen vacancies (V_0) is thus created around the gold particles decreasing the possibility of interaction with oxygen. Finally, Au/CeO_2-R (not shown) exhibits a large signal with one single maxima at 2108 cm^{-1}, showing that reduction at 300 °C further increases the number of V_0 and thus further lowers the number of O-Au peripheral adsorption sites for CO.

The DRIFT spectra of CuO/CeO_2-C and CuO/CeO_2-R essentially contain a broad and weak band spreading from 2140 to 2200 cm^{-1} due to gas phase CO (Fig. 4). CuO/CeO_2-C in particular displays only the features of gas phase CO. Adsorbed CO is not found in the calcined copper material. This suggests strong interaction between Cu and Ce [27], resulting in the presence of Cu^{2+} species, as previously suggested by XPS results [4]. CO adsorption on Cu^{2+} sites is indeed generally not observed [22,24–28,63]. On the other hand, CuO/CeO_2-R shows a weak band at 2114 cm^{-1}. The weak intensity suggests that the reducing hydrogen treatments performed at 300 °C after the synthesis and at 150 °C before the FTIR experiment may not fully reduce copper to the metallic state, in agreement with previous XPS results [4]. This may be attributed to the high reactivity and mobility of oxygen atoms of the ceria

support at these temperatures, in agreement with the kinetic results (Section 2.1).

The infrared spectra of CO adsorbed on bimetallic AuCu catalysts at around −90 °C are shown on Fig. 5. The calcined materials show two-component signals with maxima at 2103 and 2118 cm^{-1}, which are very similar in position to those observed in Au/CeO_2-C. They are assigned to CO adsorbed on Au^0 and O-Au-CO sites, respectively. In contrast, when the bimetallics are reduced, the intensity of the bands related to adsorbed CO is much higher (relative to gas phase CO) than for the calcined samples (see Fig. 5, the black line). The signal consists in a two-band feature, like in the calcined catalysts, positioned at 2105 and 2125 cm^{-1}.

The intensity ratio of the high vs. low wavenumber band (at 2125 cm^{-1}) is higher than in any other sample; it is also significantly shifted, by +5–8 cm^{-1}, as compared to the high wavenumber component of the CO adsorption feature in other calcined (2117–2118 cm^{-1}, Fig. 5) and reduced (2120 cm^{-1}, Fig. 4) systems. Hence, this band appears as a specificity of the reduced bimetallic Au_1Cu_1/CeO_2 sample. It has been attributed to metallic Cu^0 in SBA-15 supported AuCu alloys [3,11] and to Cu^0 or Cu^+ in alumina-supported AuCu alloys [6]. The large blue shift, as compared with typical wavenumbers of Cu^0-CO sites (<2100 cm^{-1}), however suggests that the related Cu adsorption sites are electron deficient, in agreement with previous XPS results [4]. Given the high electronegativity of gold, copper atoms can be made electron deficient if they are in direct contact with gold atoms, e.g. if they are alloyed with gold atoms in particular. In this case, an electron transfer directed toward gold may indeed occur between Au and Cu, making copper atoms deficient in electrons. Hence, since the presence of AuCu alloys in Au_1Cu_1/CeO_2-R was previously evidenced [4], the band at 2125 cm^{-1} is more specifically attributed to CO adsorbed on alloyed copper atoms. The site is formalized as Au-Cu^+ in the following in order to account for the electron deficient Cu, in agreement both with XPS results [4] and with the relatively high stability under oxygen of the related carbonyl species (see Section 3.2.2 below), which is typical of Cu^+ carbonyl species [21,27,64]. On the other hand, the low wavenumber band (at 2105 cm^{-1}) is attributed to the corresponding electron-rich, Cu-alloyed Au atoms. The similarity in position with the Au^0–CO species found in Au/CeO_2-R* (Fig. 4, 2105 cm^{-1}) suggests that the red-shift expected for the $Au^{\delta-}$–CO species is counterbalanced by the lower number of such species, due to the replacement of Au surface atoms with Cu in the alloyed system. In summary, the two CO adsorption bands observed at −90 °C on Au_1Cu_1/CeO_2-R catalyst are ascribed to $Au^{\delta-}$–CO (2105 cm^{-1}) and Au-Cu^+–CO (2125 cm^{-1}). A schematic representation of all the CO adsorption sites detected by DRIFT in the various gold-copper-ceria systems studied here can be found in Scheme 1.

3.2.2. Stability and reactivity of adsorbed CO in the calcined materials

In order to determine the thermal stabilities of CO species adsorbed on gold sites (Au^0–CO and O-Au^0–CO), desorption of adsorbed CO was investigated as function of temperature on Au/CeO_2–C and Au_1Cu_1/CeO_2–C. After CO adsorption reaches the maximum (plateau), 4% CO/He flow was switched off and the temperature was allowed to increase. Fig. 6a shows the two-band feature initially present over Au/CeO_2-C at −90 °C (Fig. 4), which corresponds to the two Au^0 and O-Au adsorption sites. Both bands persist in the same positions and in a similar intensity ratio up to −40 °C. With further temperature increase, at −20 °C, the IR band of Au^0-CO (2103 cm^{-1}) disappears, while the band of O-Au-CO (2117 cm^{-1}) decreases. Note that the decrease in intensity is accompanied by a blue shift in the position of the band, as expected from the decrease in surface coverage [18]. Finally, the band at 2117 cm^{-1} disappears at room temperature, indicating weak CO adsorption on gold sites, in agreement with the low adsorption energies (−0.34 to −0.17 eV) calculated by DFT [65]. The higher persistence of the band at 2117 cm^{-1} confirms the stronger adsorption of CO on the perimeter O-Au-CO site, rather than on purely metallic gold atoms of the particle.

On the copper-containing sample (Fig. 6b), both bands corresponding to the Au^0-CO and O-Au-CO species (initially at 2103 cm^{-1} and 2118 cm^{-1}, respectively) co-exist in a similar intensity ratio up to −10 °C. The overall CO coverage however starts to decrease with increasing temperature from about −60 °C, as indicated by the blue shift observed in the position of both bands at all temperatures above −60 °C. Both bands disappear when the temperature reaches 0 °C. The presence of copper thus appears to somewhat stabilize the Au^0-CO species vs. the interface site at higher temperature (−10 °C) than in the Cu-free sample (in which it is lost between −40 °C and −20 °C).

It is interesting that both species are stable upon introduction of O_2 at −90 °C. The intensities of CO adsorbed on Au^0 (2103 cm^{-1}) and on O-Au (2118 cm^{-1}) sites are indeed unchanged up to 34 min of CO-O_2 interaction (Fig. 7). The intensities of physisorbed CO_2 (2340 cm^{-1}) also remain unchanged. Note that the same intensity of adsorbed CO_2 was observed before the inlet of O_2. This suggests that CO_2 is produced by a reaction between adsorbed CO and lattice oxygen. The absence of reaction between adsorbed CO and the continuous supply of oxygen indicates that oxygen is not activated over Au_1Cu_1/CeO_2–C at −90 °C, neither over an oxygen vacancy of the ceria support (Mars Van Krevelen mechanism), nor via an Eley-Rideal mechanism. Besides, the stability of both Au^0-CO and O-Au-CO species under oxygen indicates that none of the CO adsorption sites qualifies as oxygen activation site.

3.2.3. Specific reactivity of adsorbed CO in the reduced Au_1Cu_1/CeO_2-R catalyst

For Au_1Cu_1/CeO_2-R, the FTIR spectra of CO-O_2 interaction as a function of reaction time (Fig. 8) are significantly different from those of Au_1Cu_1/CeO_2–C. In the reduced bimetallic catalyst, the intensity of adsorbed CO_2 increases with time under oxygen, showing that the oxidation of CO readily occurs at −90 °C on this material. Besides, this is concomitant with a decrease in the intensities of both adsorbed CO bands (at 2105 and 2125 cm^{-1}). It is noted also that virtually no carbonates accumulate on the catalyst surface in the process (Fig. 8b), as shown by the lower relative intensities of the carbonates signals vs. the CO_2 signal, as compared with Au_1Cu_1/CeO_2–C (Fig. 7). The relative intensities of adsorbed CO and CO_2 are plotted against time under oxygen in Fig. 9. It clearly shows that the production of adsorbed CO_2 gradually increases, as the intensities of adsorbed CO on both Au^0 (2105 cm^{-1}) and Au-Cu^+ (2125 cm^{-1}) sites decrease with increasing CO-O_2 interaction time. It suggests that molecular oxygen is activated and allowed to react possibly with one of the two observed adsorbed CO species to produce CO_2. It is interesting that very different disappearance kinetics are observed for each species: the disappearance of CO adsorbed on Au^0 is significantly faster than the disappearance of CO adsorbed on Au-Cu^+. It may suggest that CO_2 is formed by consuming Au^0-CO sites; Au^0 would thus be the active site for CO oxidation in Au_1Cu_1/CeO_2-R. The adsorption energy of CO on metallic gold is indeed quite low, even on the corner and edge sites of the particle [66]. Besides, the partial reaction order in CO is similar in Au_1Cu_1/CeO_2–R and in Au/CeO_2–C (0.34–0.38, Table 1), suggesting that the surface site responsible for CO activation is similar in both systems. Given that the Au^0-CO species can be found in both materials and that it is the only CO species that the two materials have in common (Fig. 5), we can reasonably propose it as one active site for CO oxidation in Au_1Cu_1/CeO_2–R, in agreement with results reported by Liu et al. [3]. The role of the Au-Cu^+–CO species is not clear. It may contribute to CO oxidation by providing additional sites for CO adsorption. However its

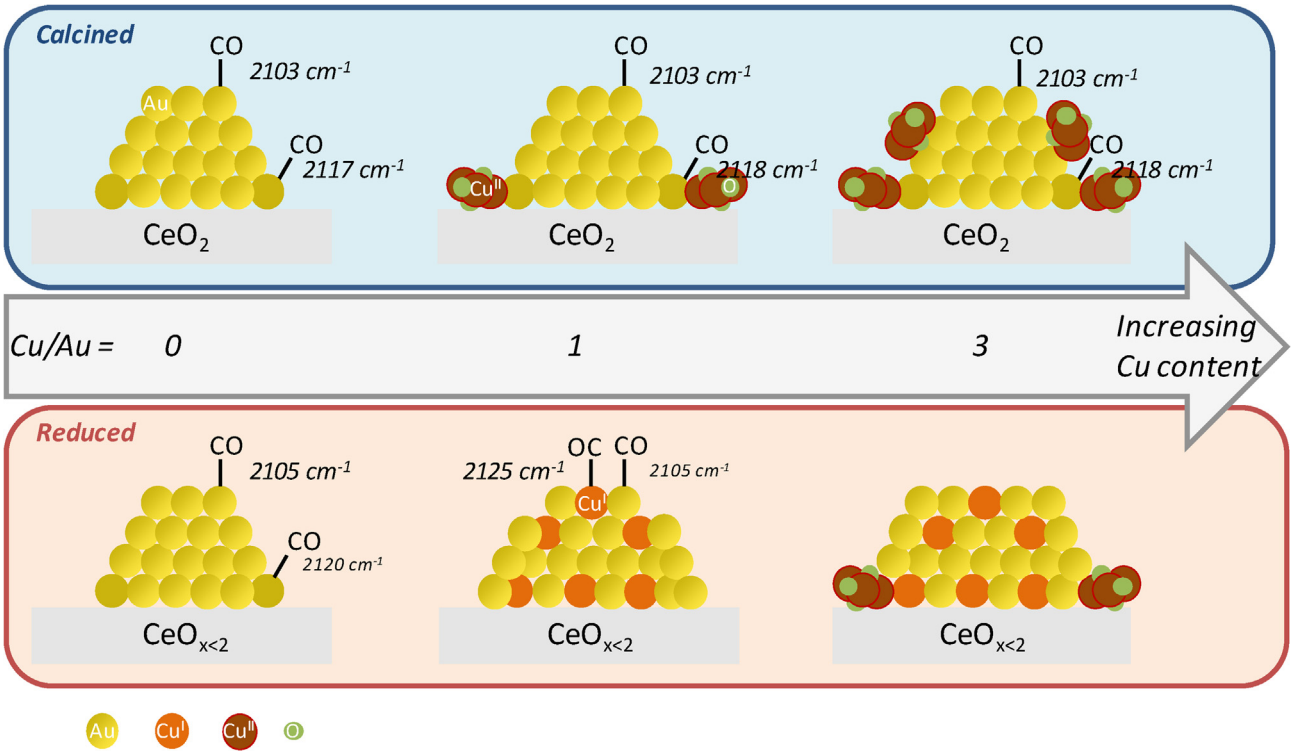

Scheme 1. Summary of the possible configurations of the AuCu/CeO_2 system and of the various CO adsorption sites detected by DRIFT, as a function of the Cu/Au ratio and pre-treatment conditions.

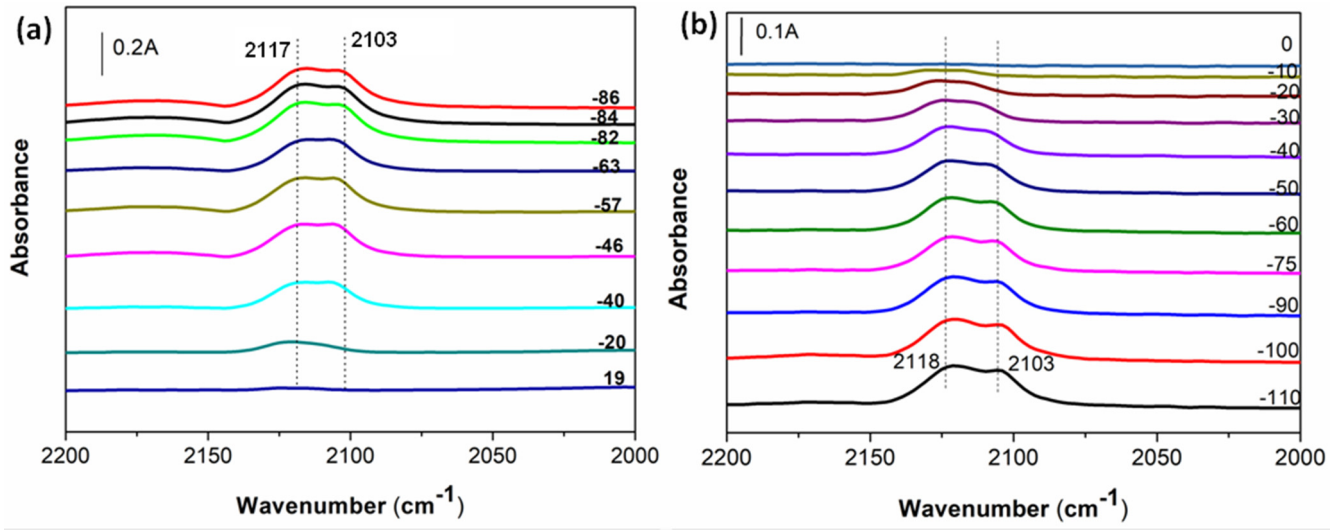

Fig. 6. Evolution of FTIR spectra of adsorbed CO species on Au/CeO_2-C (a) and on Au_1Cu_1/CeO_2-C (b) as a function of temperature (shown on top of each spectrum, in °C).

disappearance may also result from the transformation of the surface site under oxidative conditions, such as slow oxidation of the AuCu surface alloy (ultimately resulting in the formation of Au and CuO sites) or simple displacement of adsorbed CO by adsorbed O_2 on the Au-Cu^+ site. Kinetic studies indeed clearly show that the superiority of Au_1Cu_1/CeO_2–R results from a much more efficient activation of the oxygen molecule (Table 1, Fig. 3, Section 2.1). The involvement of the Au-Cu^+ site, which is specific to the reduced bimetallic catalyst, in oxygen activation is thus likely.

In order to get potential insight into the type of sites which are active for oxygen activation on Au_1Cu_1/CeO_2–R, competition experiments have been performed, since direct observation of adsorbed oxygen is not possible by FTIR. In these experiments, oxygen is introduced first and the FTIR spectrum acquired immediately after CO introduction at −90 °C. For comparison, the same experiment is performed by admitting first CO and then O_2.

Fig. 10 shows the effect of the adsorption sequence of CO and O_2 on the FTIR spectra of Au_1Cu_1/CeO_2-R. The CO-CO_2 region of the spectra looks the same, whether CO is introduced before O_2 or vice-versa, and the positions of bands corresponding to adsorbed CO and adsorbed CO_2 are unchanged. This is in marked contrast with the shifts in CO adsorption bands observed on Au/TiO_2 at 90 K [18], which were attributed to competitive CO and O_2 adsorption on Au step sites. Besides, the intensities of bands, and in

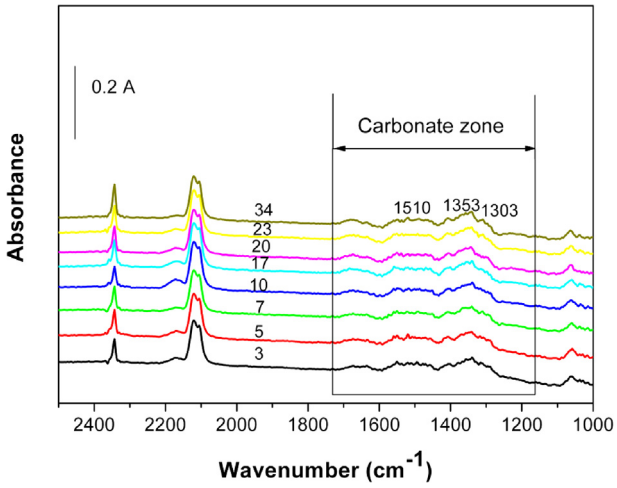

Fig. 7. Time evolution of the CO stretching and carbonate regions, after switching the flow from 4% CO/He to 20% O_2/He at −90 °C for Au_1Cu_1/CeO_2–C. Values in minutes are shown on top of each spectrum.

particular that of adsorbed CO_2, are higher when O_2 is introduced before CO (Fig. 10). This implies either that oxygen does not adsorb on CO adsorption sites (which is likely for the Au^0 site given that apparent activation energy for oxygen adsorption ≫ apparent activation energy for CO adsorption and given that Au_1Cu_1/CeO_2-C is not active at −90 °C, Fig. 7), or that if it does (which could be the case for Au-Cu^+), it is easily displaced by CO. Besides, pre-adsorbed oxygen favors the formation of CO_2, i.e. the catalytic oxidation of CO. On the other hand, pre-adsorbed CO slightly inhibits the formation of CO_2 and thus the catalytic reaction between CO and O_2. This is consistent with the postulate that Au-Cu^+ is the oxygen activation site. Indeed, when oxygen is introduced first, it may readily react with a free Au-Cu^+ surface site and carry out the oxidation of CO as soon as CO is introduced and activated on a free Au^0 surface site. On the other hand, when CO is introduced first, it will react with both Au^0 and Au-Cu^+ surface sites (2105 and 2125 cm^{-1}, Fig. 5). The Au-Cu^+ surface site is thus no longer available and oxygen will thus first need to displace CO from this site before it can be activated, which may delay CO oxidation and thus CO_2 formation. Such a competition between CO and O_2 for the Au-Cu^+ adsorption site might also account for the high oxygen reaction order observed over this catalyst, since CO and O_2 are introduced simultaneously in the catalytic experiments (Table 1).

3.3. Discussion

All FTIR results point to the fact that adsorbed CO reacts with adsorbed O_2 to produce CO_2. It is generally accepted that, when the gold-catalyzed CO oxidation involves reducible oxides (MO_x), such as ceria, as catalyst support, CO and O_2 adsorption occur on two different types of sites via a Langmuir-Hinshelwood model involving CO adsorbed on Au that reacts with oxygen activated at the Au-MO_x interface [16,17,19]. In our case, considering the redox properties of Cu and the possible contribution of Au-Cu^+ as adsorption site, we propose that oxygen adsorbs on the highly electron-deficient alloyed Cu site (rather than on an oxygen vacancy of the ceria support in Au/CeO_2), while CO is adsorbed on Au^0, and that they readily react following a Langmuir-Hinshelwood mechanism (instead of the Mars-Van Krevelen observed with Cu/CeO_2) at all the neighboring Au^0/Au-Cu^+ interfaces available in the AuCu solid solution. Such active sites, which can be found over the whole hemispherical particle surface, are more numerous than the Au/CeO_2 interfaces involved in the Au/CeO_2-catalyzed CO oxidation, which are exclusively located at the perimeter of the gold nanoparticle. It is noted that the oxidation of CO catalyzed by Au/CeO_2-based systems is known to be poorly sensitive to the presence of hydrogen in the feed [50], as confirmed by the similar kinetics observed in the absence and in the presence of hydrogen (this work, Section 3.1). Hence, support-mediated oxygen activation prevails over Au/CeO_2 under PROX conditions. The contribution of hydrogen-mediated oxygen activation [67] is minimal over ceria-based gold catalysts, despite the hydrogen-rich conditions of the PROX, due to the specificity of the ceria support [50]. The higher activity of Au_1Cu_1/CeO_2-R vs. Au/CeO_2 may thus be accounted for by the higher number of active sites found in the bimetallic catalyst. Such active sites are also more numerous in the stoichiometric alloy rather than in any other Au/Cu compositions, which is consistent with the superior activity of Au_1Cu_1/CeO_2-R vs. $AuCu/CeO_2$-R with other Au/Cu ratios (Table 1, [4]).

Hence, the intimate mixture between Au and Cu atoms creates a new and abundant adsorption site for oxygen activation, which is the closest possible to CO adsorption sites and which ensures fast CO oxidation. In this configuration, the Au/CeO_2 interface becomes less relevant to the reaction and the possible presence of not fully

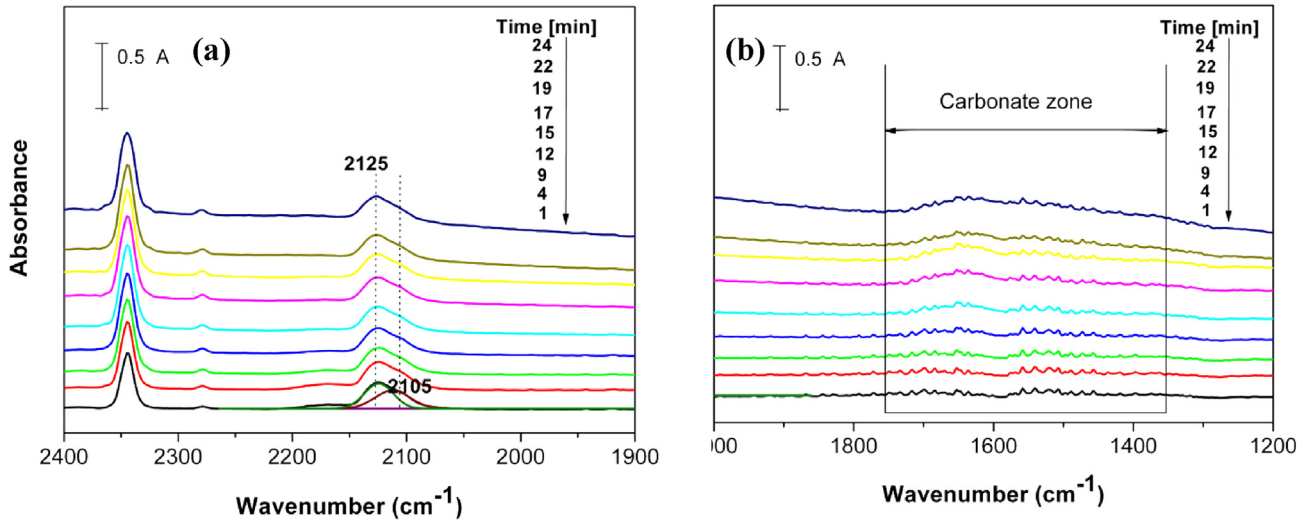

Fig. 8. Time evolution of (a) the CO stretching region and (b) the carbonate region, after the flow switch from 4% CO/He to 20% O_2/He at −90 °C for Au_1Cu_1/CeO_2-R.

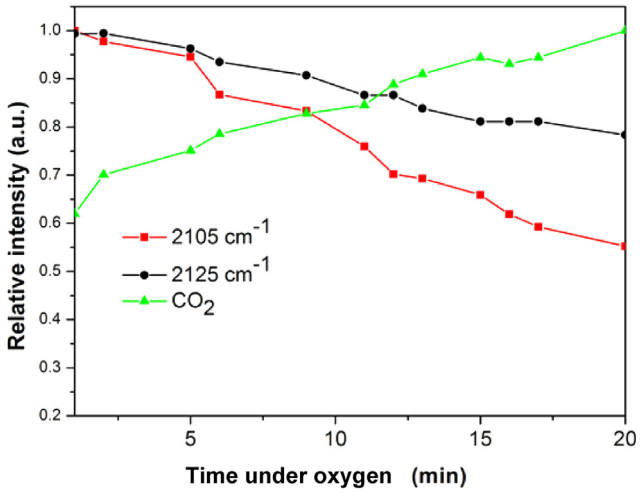

Fig. 9. Plots of the relative intensities of adsorbed CO sites and CO_2 (2340 cm^{-1}) on Au_1Cu_1/CeO_2-R catalyst as function of CO-O_2 interaction time.

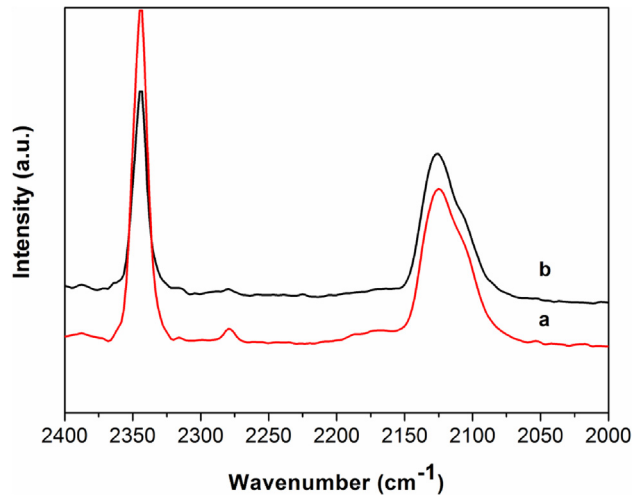

Fig. 10. FTIR spectra of adsorbed CO and CO_2 species on Au_1Cu_1/CeO_2-R. (a) preadsorbed 20%O_2/He at −90 °C, followed by admission of 4%CO/He at −90 °C, (b) admission of 20%O_2/He on pre-adsorbed 4%CO/He at −90 °C.

reduced CuO_x species in that location [3] thus does not hinder the reaction as it may do in the calcined materials. The intimate mixing of O_2 activation sites (Au-Cu^+) amongst CO adsorption sites (Au^0) is more efficient towards CO oxidation than both ceria-mediated and CuO_x-mediated oxygen activations, in which only the periphery of the gold nanoparticle is active, regardless of how large (extended ceria support) or how localized (CuO_x islands in the vicinity of the gold particles) the reducible oxide is [68].

4. Conclusions

Kinetic and DRIFT studies have been performed for the first time on ceria-supported AuCu PROX catalysts, in the 100–150 °C and −90–25 °C temperature ranges, respectively. The values of apparent activation energies are intermediate to those found for the Au/CeO_2- (40 kJ/mol) and Cu/CeO_2- (83 kJ/mol) catalyzed PROX processes, regardless of the treatment (calcination or reduction) of the bimetallic catalyst and the Cu/Au ratio considered (stoichiometric or 3). The reduced catalysts however systematically display lower activation energy (43 ± 3 kJ/mol) than their calcined counter-parts (57 ± 7 kJ/mol), as well as significantly lower CO reaction orders and higher O_2 reaction orders. O_2 reaction orders in particular are much higher than those found for Au/CeO_2-catalyzed PROX, regardless of the temperature. Furthermore, in the reduced state, the stoichiometric alloy composition allows to switch from a rate-determining step in which CO is involved ($\beta_{O2} < \alpha_{CO}$) to a rate-determining step in which oxygen is involved ($\beta_{O2} > \alpha_{CO}$), while activation energy and CO reaction order remain similar to the Au/CeO_2-catalyzed process. DRIFT study of the reduced Au_1Cu_1/CeO_2 catalyst shows the presence of a specific component at 2125 cm^{-1}, which is attributed to CO adsorption on electron-deficient, gold-alloyed copper atoms. Hence, while calcined catalysts essentially show screening of the catalytic properties of Au by Cu and disruption of the Au/CeO_2 interface, the reduced catalysts demonstrate a real synergy between Au and Cu. Results of the CO-O_2 interaction study further show that Au_1Cu_1/CeO_2-R is active for CO oxidation at −90 °C. The fact that preadsorption of O_2 enhances the rate of CO_2 formation suggests that CO oxidation results from a reaction between adsorbed CO and adsorbed O_2 and that O_2 is adsorbed on a site that is active for CO adsorption but is not involved in CO activation. A Langmuir-Hinshelwood mechanism involving CO adsorbed on Au^0 (2103–2108 cm^{-1}) which reacts within the same AuCu solid solution particle with oxygen adsorbed on Au-Cu^+ sites (2125 cm^{-1}) is proposed. By maximizing the number of CO*/O* interfaces, the dilution of oxygen activation sites amongst CO activation sites may account for the higher PROX efficiency of Au_1Cu_1/CeO_2-R.

Declaration of Competing Interest

The authors declare that they have no known competing financial interests or personal relationships that could have appeared to influence the work reported in this paper.

Acknowledgements

We gratefully acknowledge financial support from the Open Research Subject of the Control and Safety Key Laboratory of Sichuan Province (Research Base) (grant No. szjj2017-075), the National Natural Science Foundation of China (NSFC, grant No. 21706216) and the Open Research Subject of the Key Laboratory (Research Base) of Food Engineering of Sichuan Province (grant No. szjj2017-109). X. Liao acknowledges the financial support of young scholar in Xihua University. Dr. Wei Xie (Kyushu University, Japan) and Yanan Zhou (Sichuan University) are thanked for fruitful discussions. Dr. Fangli Jing (Sichuan University) is thanked for reading the manuscript. Alain Rach and Fabrice Vigneron (ICPEES/CNRS) are thanked for technical support on the catalytic set-up.

References

[1] T.S. Mozer, D.A. Dziuba, C.T.P. Vieira, F.B. Passos, J. Power Sources 187 (2009) 209–215.
[2] J.C. Bauer, D. Mullins, M.J. Li, Z.L. Wu, E.A. Payzant, S.H. Overbury, S. Dai, Phys. Chem. Chem. Phys. 13 (2011) 2571–2581.
[3] X.Y. Liu, A.Q. Wang, L. Li, T. Zhang, C.Y. Mou, J.F. Lee, J. Catal. 278 (2011) 288–296.
[4] X.M. Liao, W. Chu, X.Y. Dai, V. Pitchon, Appl. Catal. B 142 (2013) 25–37.
[5] R. Fiorenza, C. Crisafulli, G.G. Condorelli, F. Lupo, S. Scire, Catal. Lett. 145 (2015) 1691–1702.
[6] S. Najafishirtari, R. Brescia, P. Guardia, S. Marras, L. Manna, M. Colombo, ACS Catal. 5 (2015) 2154–2163.
[7] S.A. Nikolaev, E.V. Golubina, I.N. Krotova, M.I. Shilina, A.V. Chistyakov, V.V. Kriventsov, Appl. Catal. B 168 (2015) 303–312.
[8] R. Fiorenza, C. Crisafulli, S. Scire, Int. J. Hydrog. En. 41 (2016) 19390–19398.
[9] X.M. Liao, V. Caps, W. Chu, V. Pitchon, RSC Adv. 6 (2016) 4899–4907.
[10] N. Zanganeh, V.K. Guda, H. Toghiani, J.M. Keith, ACS Appl. Mater. Inter. 10 (2018) 4776–4785.
[11] X. Li, S.S.S. Fang, J. Teo, Y.L. Foo, A. Borgna, M. Lin, Z.Y. Zhong, ACS Catal. 2 (2012) 360–369.

[12] W.C. Zhan, J.L. Wang, H.F. Wang, J.S. Zhang, X.F. Liu, P.F. Zhang, M.F. Chi, Y.L. Guo, Y. Guo, G.Z. Lu, S.H. Sun, S. Dai, H.Y. Zhu, J. Am. Chem. Soc. 139 (2017) 8846–8854.
[13] S. Najafishirtari, T.M. Kokumai, S. Marras, P. Destro, M. Prato, A. Scarpellini, R. Brescia, A. Lak, T. Pellegrino, D. Zanchet, L. Manna, M. Colombo, ACS Appl. Mater. Inter. 8 (2016) 28624–28632.
[14] C.X. Qi, Y.H. Zheng, H. Lin, H.J. Su, X. Sun, L.B. Sun, Appl. Catal. B 253 (2019) 160–169.
[15] F. Boccuzzi, A. Chiorino, S. Tsubota, M. Haruta, J. Phys. Chem. 100 (1996) 3625–3631.
[16] M.A. Bollinger, M.A. Vannice, Appl. Catal. B 8 (1996) 417–443.
[17] F. Boccuzzi, G. Cerrato, F. Pinna, G. Strukul, J. Phys. Chem. B 102 (1998) 5733–5736.
[18] F. Boccuzzi, A. Chiorino, J. Phys. Chem. B 104 (2000) 5414–5416.
[19] B.K. Chang, B.W. Jang, S. Dai, S.H. Overbury, J. Catal. 236 (2005) 392–400.
[20] A. Chiorino, M. Manzoli, F. Menegazzo, M. Signoretto, F. Vindigni, F. Pinna, F. Boccuzzi, J. Catal. 262 (2009) 169–176.
[21] A. Davo-Quinonero, M. Navlani-Garcia, D. Lozano-Castello, A. Bueno-Lopez, J.A. Anderson, ACS Catal. 6 (2016) 1723–1731.
[22] D. Gamarra, A. Martinez-Arias, J. Catal. 263 (2009) 189–195.
[23] D. Gamarra, C. Belver, M. Fernandez-Garcia, A. Martinez-Arias, J. Am. Chem. Soc. 129 (2007) 12064.
[24] A. Hornes, P. Bera, A.L. Camara, D. Gamarra, G. Munuera, A. Martinez-Arias, J. Catal. 268 (2009) 367–375.
[25] A. Martinez-Arias, D. Gamarra, M. Fernandez-Garcia, A. Hornes, P. Bera, Z. Koppany, Z. Schay, Catal. Today 143 (2009) 211–217.
[26] A. Martinez-Arias, M. Fernandez-Garcia, O. Galvez, J.M. Coronado, J.A. Anderson, J.C. Conesa, J. Soria, G. Munuera, J. Catal. 195 (2000) 207–216.
[27] A. Martinez-Arias, M. Fernandez-Garcia, J. Soria, J.C. Conesa, J. Catal. 182 (1999) 367–377.
[28] A. Martinez-Arias, D. Gamarra, M. Fernandez-Garcia, A. Hornes, C. Belver, Top. Catal. 52 (2009) 1425–1432.
[29] M.M. Schubert, V. Plzak, J. Garche, R.J. Behm, Catal. Lett. 76 (2001) 143–150.
[30] K. Liu, A.Q. Wang, T. Zhang, ACS Catal. 2 (2012) 1165–1178.
[31] M. Manzoli, F. Boccuzzi, A. Chiorino, F. Vindigni, W.L. Deng, M. Flytzani-Stephanopoulos, J. Catal. 245 (2007) 308–315.
[32] G. Avgouropoulos, M. Manzoli, F. Boccuzzi, T. Tabakova, J. Papavasiliou, T. Ioannides, V. Idakiev, J. Catal. 256 (2008) 237–247.
[33] G. Sedmak, S. Hocevar, J. Levec, J. Catal. 213 (2003) 135–150.
[34] T. Caputo, L. Lisi, R. Pirone, G. Russo, Ind. Eng. Chem. Res. 46 (2007) 6793–6800.
[35] H.C. Lee, D.H. Kim, Catal. Today 132 (2008) 109–116.
[36] M. Moreno, G.T. Baronetti, M.A. Laborde, F.J. Marino, Int. J. Hydrog. En. 33 (2008) 3538–3542.
[37] J.L. Ayastuy, A. Gurbani, M.P. Gonzalez-Marcos, M.A. Gutierrez-Ortiz, Ind. Eng. Chem. Res. 48 (2009) 5633–5641.
[38] M.J. Kahlich, H.A. Gasteiger, R.J. Behm, J. Catal. 182 (1999) 430–440.
[39] B. Schumacher, Y. Denkwitz, V. Plzak, M. Kinne, R.J. Behm, J. Catal. 224 (2004) 449–462.
[40] E. Quinet, L. Piccolo, H. Daly, F.C. Meunier, F. Morfin, A. Valcarcel, F. Diehl, P. Avenier, V. Caps, J.L. Rousset, Catal. Today 138 (2008) 43–49.
[41] Y. Denkwitz, B. Schumacher, G. Kucerova, R.J. Behm, J. Catal. 267 (2009) 78–88.
[42] T. Davran-Candan, M. Demir, R. Yildirim, React. Kinet. Mech. Cat. 104 (2011) 389–398.
[43] E. Quinet, F. Morfin, F. Diehl, P. Avenier, V. Caps, J.L. Rousset, Appl. Catal. B 80 (2008) 195–201.
[44] E. Quinet, L. Piccolo, F. Morfin, P. Avenier, F. Diehl, V. Caps, J.L. Rousset, J. Catal. 268 (2009) 384–389.
[45] Y. Azizi, C. Petit, V. Pitchon, J. Catal. 269 (2010) 26–32.
[46] S. Ivanova, V. Pitchon, C. Petit, J. Mol. Catal A 256 (2006) 278–283.
[47] S.D. Lin, M. Bollinger, M.A. Vannice, Catal. Lett. 17 (1993) 245–262.
[48] M.M. Schubert, S. Hackenberg, A.C. van Veen, M. Muhler, V. Plzak, R.J. Behm, J. Catal. 197 (2001) 113–122.
[49] W. Liu, M. Flytzani-Stephanopoulos, J. Catal. 152 (1995) 317–332.
[50] S. Ivanova, V. Pitchon, C. Petit, V. Caps, ChemCatChem 2 (2010) 556–563.
[51] G. Avgouropoulos, T. Ioannides, Chem. Eng. J. 176 (2011) 14–21.
[52] C.G. Maciel, M.N. Belgacem, J.M. Assaf, Catal. Lett. 141 (2011) 316–321.
[53] B.D. Chandler, C.G. Long, J.D. Gilbertson, C.J. Pursell, G. Vijayaraghavan, K.J. Stevenson, J. Phys. Chem. C 114 (2010) 11498–11508.
[54] R.P. Doherty, J.M. Krafft, C. Methivier, S. Casale, H. Remita, C. Louis, C. Thomas, J. Catal. 287 (2012) 102–113.
[55] F. Boccuzzi, A. Chiorino, M. Manzoli, Surf. Sci. 502 (2002) 513–518.
[56] F. Boccuzzi, A. Chiorino, M. Manzoli, Mat. Sci. Eng. C 15 (2001) 215–217.
[57] T. Tabakova, F.B. Boccuzzi, M. Manzoli, D. Andreeva, Appl. Catal. A 252 (2003) 385–397.
[58] M. Manzoli, F. Vindigni, A. Chiorino, T. Tabakova, V. Idakiev, F. Boccuzzi, React. Kin. Catal. Lett. 91 (2007) 213–221.
[59] M. Manzoli, G. Avgouropoulos, T. Tabakova, J. Papavasiliou, T. Ioannides, F. Boccuzzi, Catal. Today 138 (2008) 239–243.
[60] T. Tabakova, M. Manzoli, F. Vindigni, V. Idakiev, F. Boccuzzi, J. Phys. Chem. A 114 (2010) 3909–3915.
[61] T. Tabakova, G. Avgouropoulos, J. Papavasiliou, M. Manzoli, F. Boccuzzi, K. Tenchev, F. Vindigni, T. Ioannides, Appl. Catal. B 101 (2011) 256–265.
[62] R. Burch, J. Catal. 71 (1981) 348–359.
[63] M. Manzoli, R. Di Monte, F. Boccuzzi, S. Coluccia, J. Kaspar, Appl. Catal. B 61 (2005) 192–205.
[64] A. Gomez-Cortes, Y. Marquez, J. Arenas-Alatorre, G. Diaz, Catal. Today 133 (2008) 743–749.
[65] L. Piccolo, D. Loffreda, F.J.C.S. Aires, C. Deranlot, Y. Jugnet, P. Sautet, J.C. Bertolini, Surf. Sci. 566 (2004) 995–1000.
[66] E. Roze, E. Quinet, V. Caps, D. Bianchi, J. Phys. Chem. C 113 (2009) 8194–8200.
[67] P. Laveille, K. Guillois, A. Tuel, C. Petit, J.M. Basset, V. Caps, Chem. Commun. 52 (2016) 3179–3182.
[68] V. Caps, S. Arrii, F. Morfin, G. Bergeret, J.L. Rousset, Faraday Discuss 138 (2008) 241–256.